Available online at www.sciencedirect.com

ScienceDirect

Journal of the European Ceramic Society 34 (2014) 4043–4052

www.elsevier.com/locate/jeurceramsoc

Investigation by neutron diffraction of texture induced by the cooling process of zirconia refractories

C. Patapy [a,*], F. Gouraud [b], M. Huger [b,*], R. Guinebretière [b,*], B. Ouladiaff [c], D. Chateigner [d], T. Chotard [b,**]

[a] LMDC-UPS-INSA Toulouse, EA 3027, 135 avenue de Rangueil, 31077 Toulouse, France
[b] SPCTS, UMR CNRS 7315, Centre Européen de la Céramique, 12 rue Atlantis, 87068 Limoges, France
[c] Institut Laue-Langevin, BP156, 6 rue Jules Horowitz, 38042 Grenoble, France
[d] CRISMAT-ENSICAEN, UMR 6508, 6 boulevard du Maréchal Juin, 14050 Caen, France

Received 17 December 2013; received in revised form 23 April 2014; accepted 16 May 2014
Available online 27 June 2014

Abstract

New fused cast refractories with a high content of zirconia have been developed to face corrosion in glass furnaces. The controlled cooling process is responsible for thermal gradients. So, thermal mismatches appear between core and edge zones of blocks. Besides, the multiphasic nature of ZrO_2 based refractories is associated to thermal mismatches during cooling. Finally, the expansive transformation of ZrO_2 can lead to stress generation.

This paper is an application of neutron diffraction to study texture generated during the cooling process of zirconia based materials. In fact, it is shown that ZrO_2 crystallographic variants have particular crystallographic texture regarding the main direction of the thermal gradient in the block. It was hypothesized that a selection of crystallographic variants could be done depending on the field stress. Tensile-compressive tests at high temperature have been done, to reproduce stress environment during the transformation of zirconia.

Keywords: Refractories; Texture; Variants; Cooling process; Neutron diffraction

1. Introduction

New compositions of refractory materials with high zirconia content have been developed. They are casted using a melting process in arc furnaces followed by a controlled cooling step in moulds. Microstructure features at room temperature are complex, with a 3D skeleton of ZrO_2 crystals surrounded by a glassy phase. The different phase transitions have been detailed elsewhere and are resumed in Fig. 1.[1] Dendrites of zirconia initially grow under the form of cubic domains (C) with primary and secondary ramifications (tree structure) and probably transform into tetragonal domains (T) at around 2300 °C. Down to 1700 °C, the mixing is not supposed to be fully solid, and nucleation-growth of zirconia dendrites is rather active. Below 1700 °C, the material can be considered as fully solid with zirconia dendrites embedded in a glassy phase. Between 1000 °C and 900 °C, the martensitic transformation of zirconia occurs, where ZrO_2 goes from tetragonal structure to monoclinic (M) one. Depending on the nature of the glassy phase (soda-siliceous or boron-siliceous for example), the refractory exhibits different thermo-mechanical behaviour,[1,2] probably due to different viscous behaviour around the T-M transition.

The glassy phase as well as the different zirconia domains are characterized by different thermal expansion coefficients. Moreover the tetragonal to monoclinic transition at about 1000 °C is associated with a large volume expansion (4%), which can generate important local strains. Thereby kinetic of the cooling stage must be minimized to limit the formation of local thermo-mechanical stresses which can lead to the damage of the material (microcracking). Different authors have studied previously the thermo mechanical behaviour of fused-cast

* Corresponding authors.
** Corresponding author. Tel.: +33 5 87 50 25 60.
E-mail addresses: patapy@insa-toulouse.fr (C. Patapy), marc.huger@unilim.fr (M. Huger), rene.guinebretiere@unilim.fr (R. Guinebretière), thierry.chotard@unilim.fr (T. Chotard).

http://dx.doi.org/10.1016/j.jeurceramsoc.2014.05.027
0955-2219/

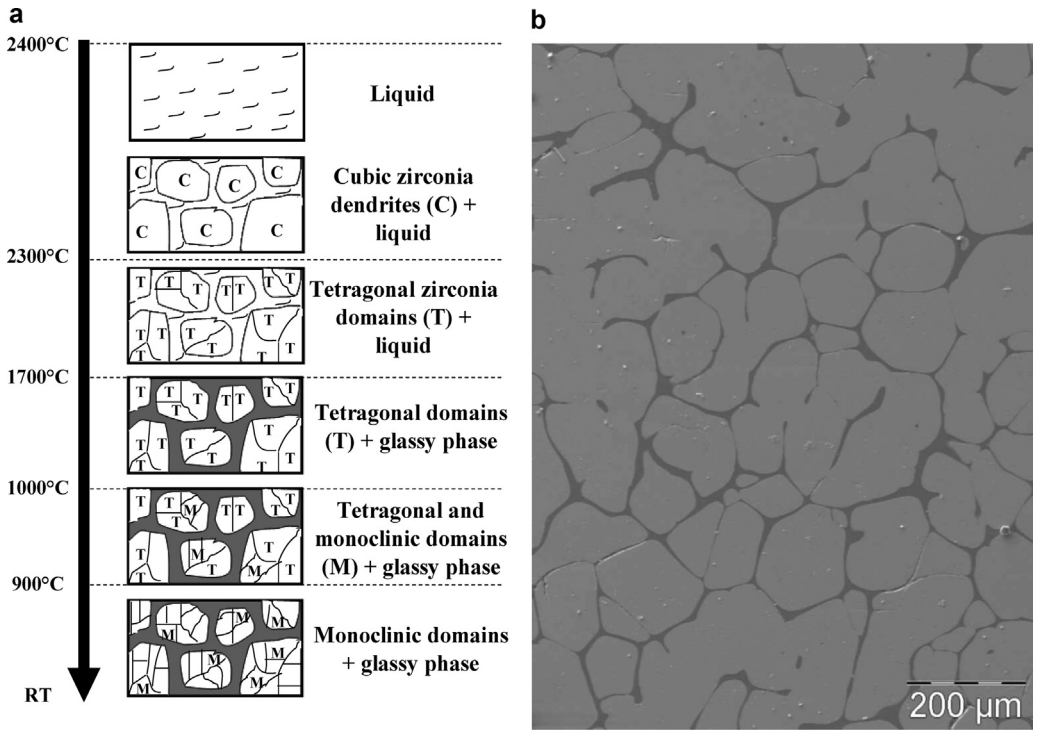

Fig. 1. Evolution of the microstructure during the cooling process (a) and final microstructure observed at room temperature by SEM (b).

refractory to avoid the appearance of important thermo mechanical stresses.[3] Cockcroft[4,5] performed a statistical analysis of macroscopic cracks in ZrO_2 refractory block and highlighted longitudinal and transverse cracks. The study showed that transversal cracks are rather due to mechanisms involved at high temperature while longitudinal ones appear below the glass transition temperature of the amorphous phase. Using conclusions of Thomas,[6] the author showed through a 3D thermo-elastic-type model, the appearance of high tensile stress after passing the T → M transformation of zirconia. In the same way, Evans[7] used a Drucker–Prager type model to study a block of Alumina–Zirconia–Silica refractory material. It was shown that passing the T → M transition in the skin area of the block is responsible for significant tensile stresses in the core, causing plastic deformation leading to its final rupture. These deformations depend on the blocksize, the transformation strains and the cooling profile. In 2000, Madi[8] computed simulation of a mesoscopic volume (some μm^3) of HZ material between 800 °C and room temperature. This model used an elastic behaviour for zirconia and a viscoplastic one for the glassy phase. A maximum level of tensile stress at the surface of the block and at interfaces between zirconia and glassy phase was measured, with interfacial debonding and cracking phenomena in the glassy phase.

Characterization of texture associated to the cooling process is of prime importance to understand stress field and damage occurrence. In-situ characterization is difficult due to high temperature conditions. Moreover crystallographic texture after cooling process in moulds has been investigated mainly for metal based materials (using X-Ray Diffraction (XRD) or Electron Backscattering Diffraction (EBSD),[9,10] but few studies are available for ceramics and especially for ZrO_2 based refractories.

Thereby crystallographic texture is studied by neutron diffraction on materials sampled in different areas of the refractory blocks. Relationships between preferential orientation of zirconia variants and main direction of thermal gradient in the block are highlighted for two different types of ZrO_2 refractories. Complementary tensile/compressive tests on samples are done during cooling to reproduce conditions of block casting. Corresponding strains are analysed to get information on the local stress field.

2. Materials

2.1. Casting process

Raw materials (zircon sand, alkali salts) are fused in electric furnaces. After refining, the molten liquid is poured into moulds before undergoing a slow controlled cooling stage. The block was cooled by adapting the external thermal conductivity with a "thermal calibrating" agent (Fig. 2).

The type of mould, geometry of blocks as well as the nature of the calibrating agent greatly influence the thermal behaviour of

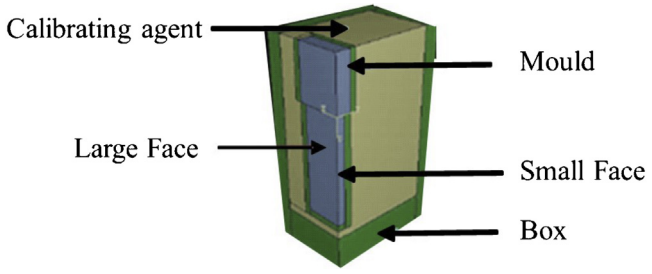

Fig. 2. Refractory block inside the mould with the presence of calibrating agent.

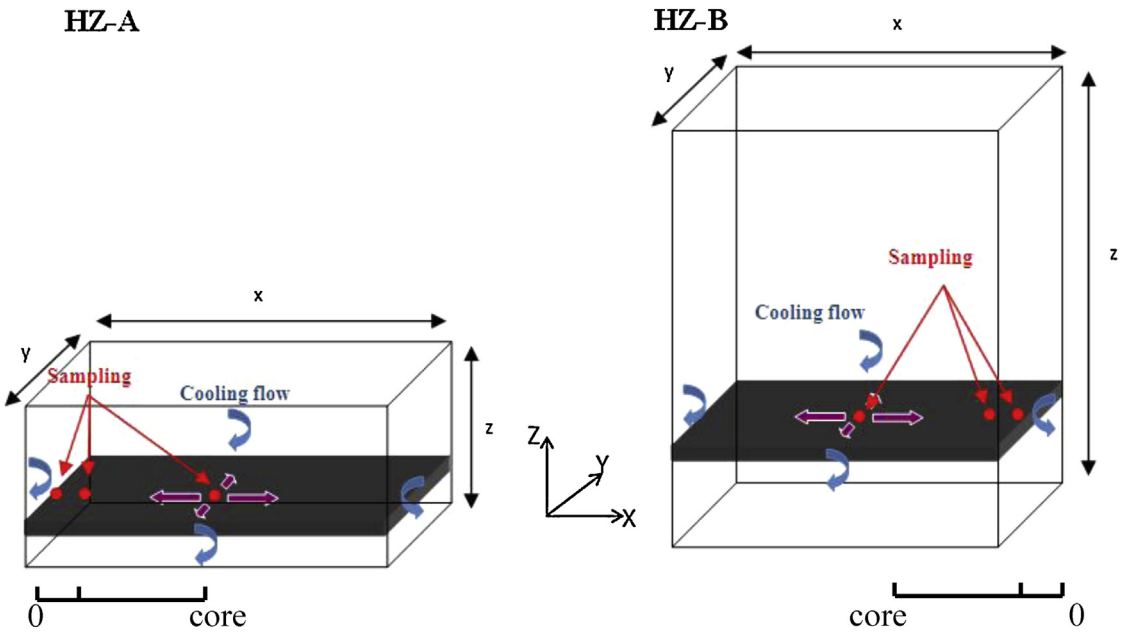

Fig. 3. Blocks and sampling zones for HZ-A and HZ-B.

the block and therefore the kinetics of cooling. Regarding their dimensions, and despite the cautious way for cooling, refractory blocks are submitted to thermal gradients between the core and the skin which cannot be completely avoided.

2.2. Sampling procedure

Two different fused-cast refractory materials (noted HZ-A and HZ-B) are studied here. They both contain 94 wt.% of zirconia dendrites surrounded by a glassy phase as illustrated in Fig. 1 Main difference is related to the difference of chemical composition of the vitreous phase which is of soda-siliceous type for HZ-A and of boron-siliceous type for HZ-B.

To investigate the impact of the cooling kinetics on crystallographic texture, cylinders were sampled at 0 and 30 mm of the edge as well as in the core of the blocks, along the *X* thermal gradient direction (Fig. 3). They were taken from two different blocks corresponding to the two different chemical composition of the glassy phase. It can be noticed that the size of the HZ-A and HZ-B blocks along the main thermal direction of gradient *X* is quite similar.

Dimensions of the samples were selected to be in accordance with the beam size of the neutron diffraction experiment.

2.3. Crystallographic variants and microstructure

Different crystallographic variants are formed during successive transformations of ZrO_2.[11] The cubic to tetragonal transformation is associated to a 45° rotation of the and $\vec{a}$ and $\vec{b}$ axis around the $\vec{c}$ axis. It induces the possible formation of three distinct crystallographic variants from one single cubic crystal. Using the pseudo-cubic lattice, axis $\vec{c_c}$ can become $\vec{a_t}$, $\vec{b_t}$ or $\vec{c_t}$. During the tetragonal to monoclinic transformation, it is possible to form 24 different crystallographic variants. In fact there are two possible orientation relationships and eight crystallographic variants for each case: $\vec{c_t} \rightarrow \vec{a_m}$ noted A, $\vec{c_t} \rightarrow \vec{b_m}$ noted B and $\vec{c_t} \rightarrow \vec{c_m}$ noted C. The monoclinic zirconia space group is P21/c and then the β angle differs from 90° (it is close to 99°). Thus considering one specific tetragonal and monoclinic respective orientations, only two crystallographic axes of the monoclinic lattice can be parallel to a tetragonal axis: the $\vec{b_m}$ axis and either the $\vec{a_m}$ or the $\vec{c_m}$ one. However, the total number of possibilities is divided by two since variants can be regrouped as equivalent crystallographic pairs by rotation of 180°around $\vec{b_m}$.[12,13] Fig. 4 illustrates for a given combination of tetragonal axes, the formation of the different monoclinic variants and their projection on pole figures 0 0 1, 0 1 0 and 0 0 1.[14]

At room temperature each zirconia dendrite is therefore constituted of different monoclinic variants. Considering the anisotropy in thermal expansion along the different crystallographic axes of the monoclinic structure, these different crystallographic variants induce thermal mismatches and then potential microcracking phenomena between variants.[15] The glassy phase within the microstructure is assumed to accommodate internal stresses induced by the anisotropic expansion mismatch between ZrO_2 grains. Nevertheless, the transformation of zirconia, combined with TE mismatches between the glassy phase and zirconia is responsible for microcracking. In absence of external stress field, variants should be present with no preferential orientation, creating a relative randomly distributed texture.

3. Experimental device

3.1. Neutron diffraction

3.1.1. Experimental set-up

Neutron diffraction is a powerful tool to study texture features on large volume samples (typically cm^3). This is of great

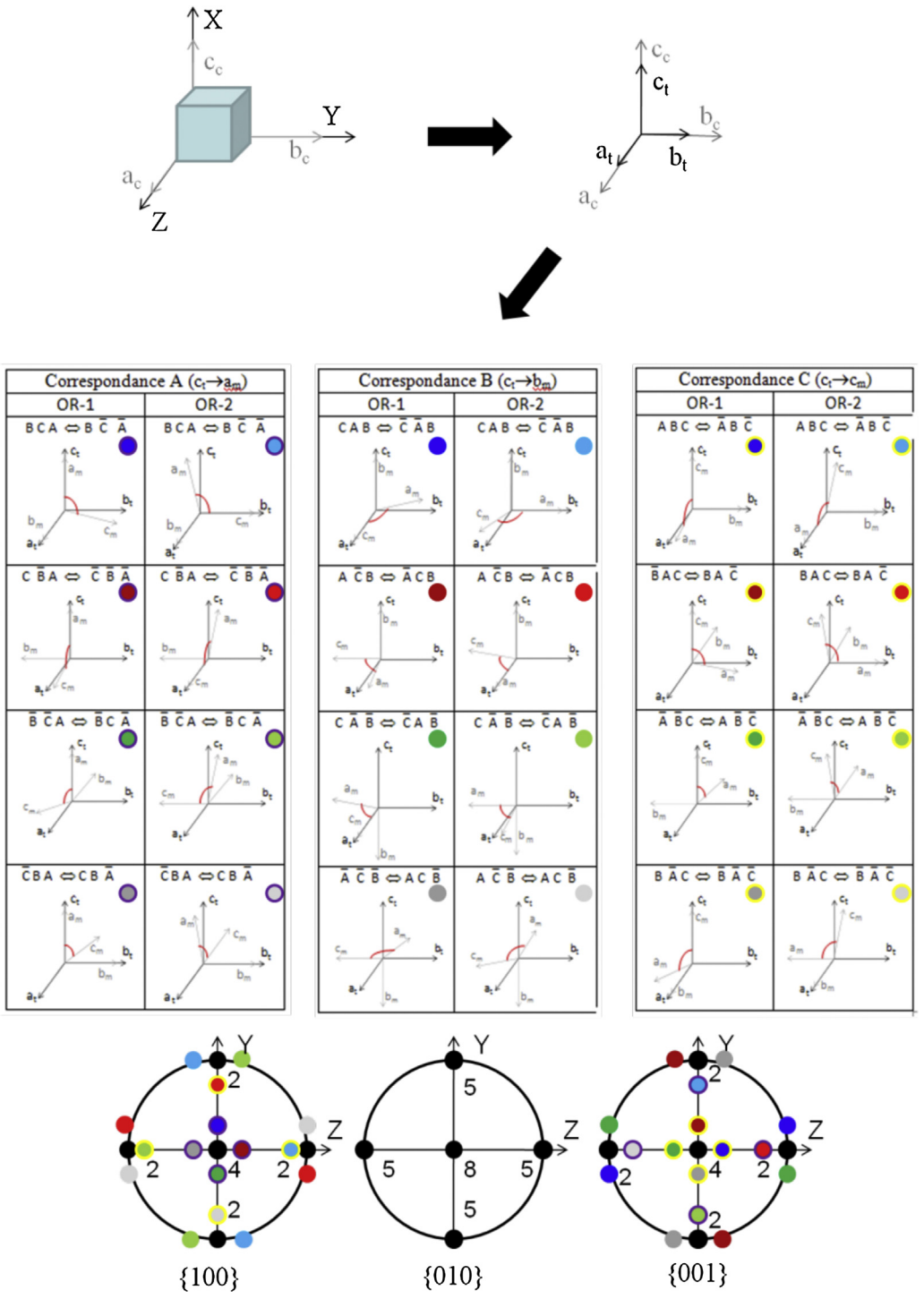

Fig. 4. Pole figures (equal area projection) obtained for a random distribution of monoclinic variants relative to a given tetragonal crystal.[14]

interest as studied materials have large grains (volume up to several hundred μm^3). Different tests were performed on the D1B line of the Institut Laue Langevin (ILL-Grenoble) with cylinders sampled in the refractory block (Fig. 3). The system installed on the line D1B is an Euler circle type diffractometer equipped with a high-intensity curve detector location covering a 2θ angular range of 80° (Fig. 5).[16,17] The radius of curvature is 1.5 m. Pyrolytic graphite monochromator is used to select the focusing beam with wavelength $\lambda = 2.52$ Å. A graphite filter removes contamination in $\lambda/2$.[18] The detector can be moved so that an angular range of $2° < 2\theta < 130°$ can be covered and resolution of 2θ angle is typically of 0.2°. Diffraction pattern with sufficient counting statistics can be collected in a few seconds on a bulk sample. Azimuth φ ($0° \rightarrow 355°$, 10° step) and tilt χ ($0° \rightarrow 90°$, 10° step) scans have been done with a two-hour recording of 15,000 counts per diagram and 360 diagrams per

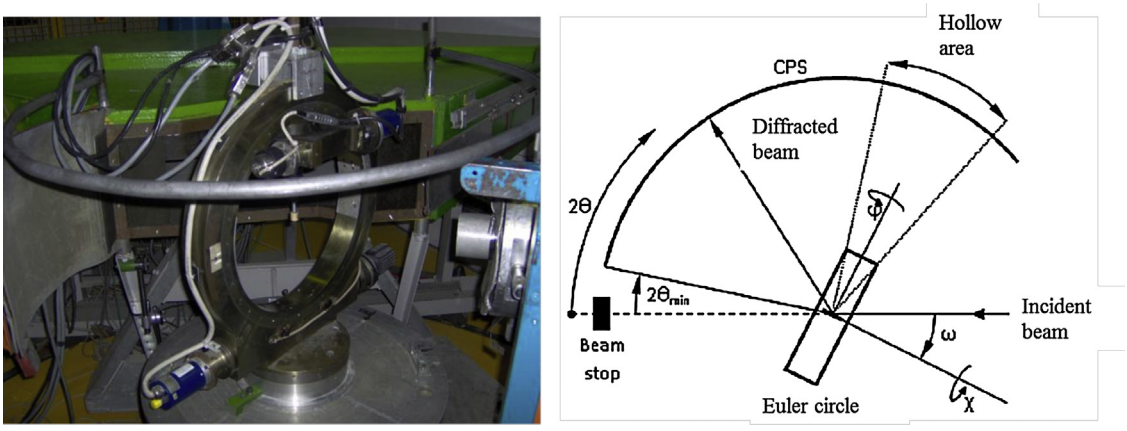

Fig. 5. Geometry of the Euler circle used on the D1B line.

test. The detector was in ω position (angle of incidence of the beam) equal to 26.3° and $\tau = 35°$ (Fig. 5). The instrument was calibrated with a standard sample of calcite.

3.1.2. Data processing

An Orientation Distribution Function (ODF) was defined and refined in the MAUD software, using the E-WIMV approach (Extended Williams–Imhoff–Matthies–Vinel)[19] based on the WIMV algorithm.[20,21] A first estimation of the ODF was calculated by replacing the geometrical average $f(g)$ obtained from values of experimental pole figures inside each element of the ODF. ODF values were then solved using an iterative algorithm of entropy maximization which includes the weighting of the reflexions (Eq. (1)).[22]

$$f^{n+1}(g) = f^{n}(g) \prod_{h=1}^{I} \prod_{m=1}^{M_h} \left(\frac{P_{\vec{h}}(\vec{y})}{P^{n}_{\vec{h}}(\vec{y})} \right)^{r_n(w_h/M_h I)} \quad (1)$$

where r_n is a relaxation parameter with $0 < r_n < 1$, M_h is the number of division points for the discretization of the integral for the whole orientations around the scattering vector of the pole figure $\rightarrow h$; w_h is the weighting of each reflexion.

Using the refined ODF, it was possible to calculate normalized pole figures for all (hkl) planes. To evaluate the reliability of the refinement, several quality factors were introduced like R_p or R_{wp}. In the same time, crystalline structure was refined using the Rietveld method.[23–25] The calculation was performed simultaneously on all the diffraction patterns and iteratively refined to couple texture analysis and structure analysis. This procedure is called combined analysis. For illustration, typical refined diffraction patterns are presented in Fig. 6.

Then, using iterative analysis of diffraction patterns obtained for the whole range of angles (φ (0° → 355°, 10° step) and χ (0° → 90°, 10° step)), pole figures were plotted using equal projection area method (Lambert projection).[25] Fig. 7 shows examples of normalized pole figures (after filtering) obtained by neutron diffraction on ferroelectric films with cubic symmetry. It can be seen that the density of clusters is maximum in the centre of the 0 0 1 pole figure (corresponding to the projection of the normal to {0 0 1} planes), and in the centre of the 100 pole figure. In a very schematic view, it can be inferred that a

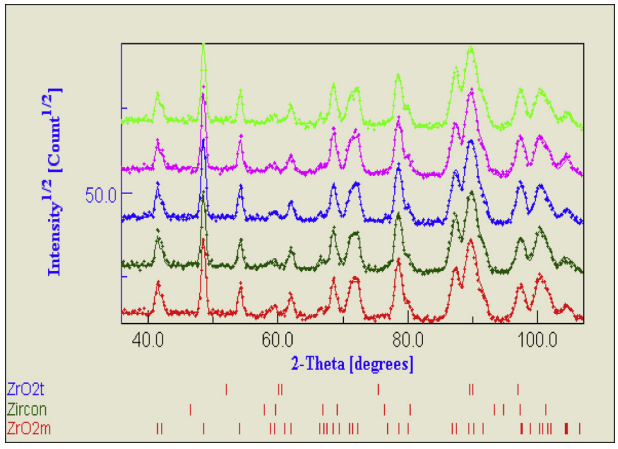

Fig. 6. Diffraction patterns obtained by neutron diffraction for HZ-A samples.

large number of planes (0 0 1) and (1 0 0) have their normal parallel with the normal to the observation plane of the sample. It describes a typical double fibre texture. For {1 1 1} pole figure, the double distribution of planes parallel to the normal of the observation plane and ones slightly inclined at 40° relative to the normal, creates both a central spot and an edged crown. The intensity of the texture is evaluated by a texture index in m.r.d. (multiple of random density), where 1 m.r.d. corresponds to a perfect random distribution.

3.2. Cooling tests under uniaxial stress

Experiments were done on large cylinder samples during cooling from 1150 °C to room temperature in order to pass

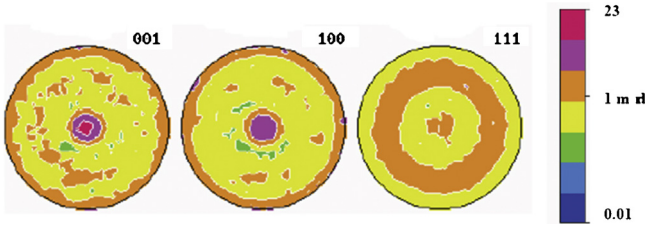

Fig. 7. Pole figures associated to {0 0 1}, {0 1 0} and {0 0 1} planes for a ferroelectric film.[26]

the T–M transition under uniaxial tensile or compressive stress. Details on the equipment developed in the SPCTS laboratory can be found elsewhere.[2,27]

4. Results

4.1. Texture associated to the cooling process

Thermal gradients are generated during the cooling process between the periphery (cooled zone) and the core of the block. Pole figures of samples collected in different zones of the blocks (respectively in periphery, at 30 mm of the edge and in the core of the block) are plotted in Fig. 8 for the two materials. The *X* direction (called main direction of thermal gradient) is kept normal to the plane of observation. One can easily identify for HZ-A samples the presence of a weak but well defined texture of {0 0 1} planes at the edge and at 30 mm from periphery. It is markedly disoriented from the centre of the figure, which is normal to the *X* direction of the temperature gradient. Projections of {1 0 0} and {0 1 0}planes draw a ring shape. It corresponds to a fiber texture of {0 0 1} planes approximately normal to the *X* direction. The low disorientation from the normal axis is probably a consequence of the sample positioning. In fact, the sample is not completely centred regarding to the width of the plate, which can induce some inclination of the thermal gradient related to the *X* direction. The pole figures of HZ-B samples obtained from periphery and 30 mm present fiber texture for {0 1 0} and {0 0 1} planes. The poles are well centred on the figure. Although the relatively low texture index (∼1.4 m.r.d.), poles corresponding to fiber texture are well defined. This analysis is confirmed by the crown periphery on the {1 0 0} pole figure.

It can be noticed for HZ-B material a 90° rotation of the {0 0 1} poles relative to the *X* axis. This rotation could be consistent with a secondary additional thermal gradient normal to the large face (Fig. 3), oriented in the direction of the block width. In the same way, the texture observed in {0 0 1} pole figure is characterized by a pole rotation which is different from 90° for HZ-A samples. This rotation could be consistent with a thermal gradient direction slightly inclined relative to the X direction, when considering a sampling zone near the bottom of the block (Fig. 3).

The neutron diffraction analysis reveals an overall fiber texture which appears to be related to the direction of the thermal gradient within the block.

If the texture was the result of a preferential crystallographic orientation in the growth of cubic germs, it could be expected to see a more pronounced texture density. On the other hand, the visco-plastic behaviour of materials (beyond 1200 °C) can probably accommodate deformations caused by potential stresses generated during Liquid → C and C → T transformations, without creating preferential orientationsof variants.

Thereby, the origin of this texture can be hypothesized as a consequence of the mechanisms involved below 1200 °C. It may be the result of a stress field (related to the main direction of thermal gradient) which existsduring the T → M transformation of zirconia. This phenomenon could lead to a preferential orientation of given monoclinic variants. This texture would be even more pronounced when the crystallographic axes of the parent domains (cubic or tetragonal) locally coincide with the direction of the thermal gradient. Indeed, for parent domains randomly oriented with respect to the gradient direction *X* (which is probably the case here), only a small proportion of these tetragonal variants (those whose crystallographic axes are relatively well aligned with the local direction of thermal gradient) will lead to a predominance of monoclinic specific variants. This hypothesis would explain partly the low density of texture measured during the test.

4.2. Effect of a supplementary heating cycle on crystallographic texture

The relationship between crystallographic texture and direction of the main thermal gradient has been shown previously. This texture is associated to the surrounding stress field when zirconia passes through the T–M transformation. In order to test the passage of the martensitic transition on texture without applied stress, samples from different positions of the refractory block were heat treated at 1500 °C. The results of the neutron diffraction experiments are presented in Fig. 9 with the observation plane normal to the *X* direction. The fiber texture ({0 0 1} planes for HZ-A; {0 1 0} and {0 0 1} planes for (HZ-B) initially aligned with the thermal gradient, is not well defined after heat treatment. In general, the texture index falls significantly and variants seem to be more randomly distributed. It can be concluded that crystallographic texture is deleted in absence of stress field when material is heat treated, confirming the role of stress environment during the T–M transformation.

4.3. Discussion on the mechanism of texture formation: evaluation of oriented local stress

A thermomechanical model using thermal (temperatures measured with thermocouples placed in different points of the moulds during the cooling process) and mechanical data (elastic properties, plastic strain associated to the T–M transformation) was used by Laurence[28] to simulate the thermomechanical behaviour of the block during cooling. The calculation of the main mechanical stress σ_{zz} during cooling in the periphery of the block was done on the "small face" using thermo-elastic modelling as illustrated in Fig. 10a. When plotting the evolution of σ_{zz} applied to the main face of the block as a function of time, it can be seen a local negative drop around the T–M transformation corresponding to a compressive state (Fig. 10a and b).

If the large face of the block is assimilated to an infinite plane, it can be supposed that the σ_{xx} stress is rather similar to σ_{zz} and exhibits a compressive state when passing the martensitic transformation of zirconia. Then, the block would be in a biaxial compressive state with a stress plane (σ_{zz} and σ_{xx}) normal to the direction of thermal gradient (*Y* for the large face), when passing the T–M transformation.

In the present study, samples have been extracted from a zone closed to the "Small face". In order to link thermomechanical results to neutron diffraction features, data obtained on the "Small face" have been extra polated to the "Large face",

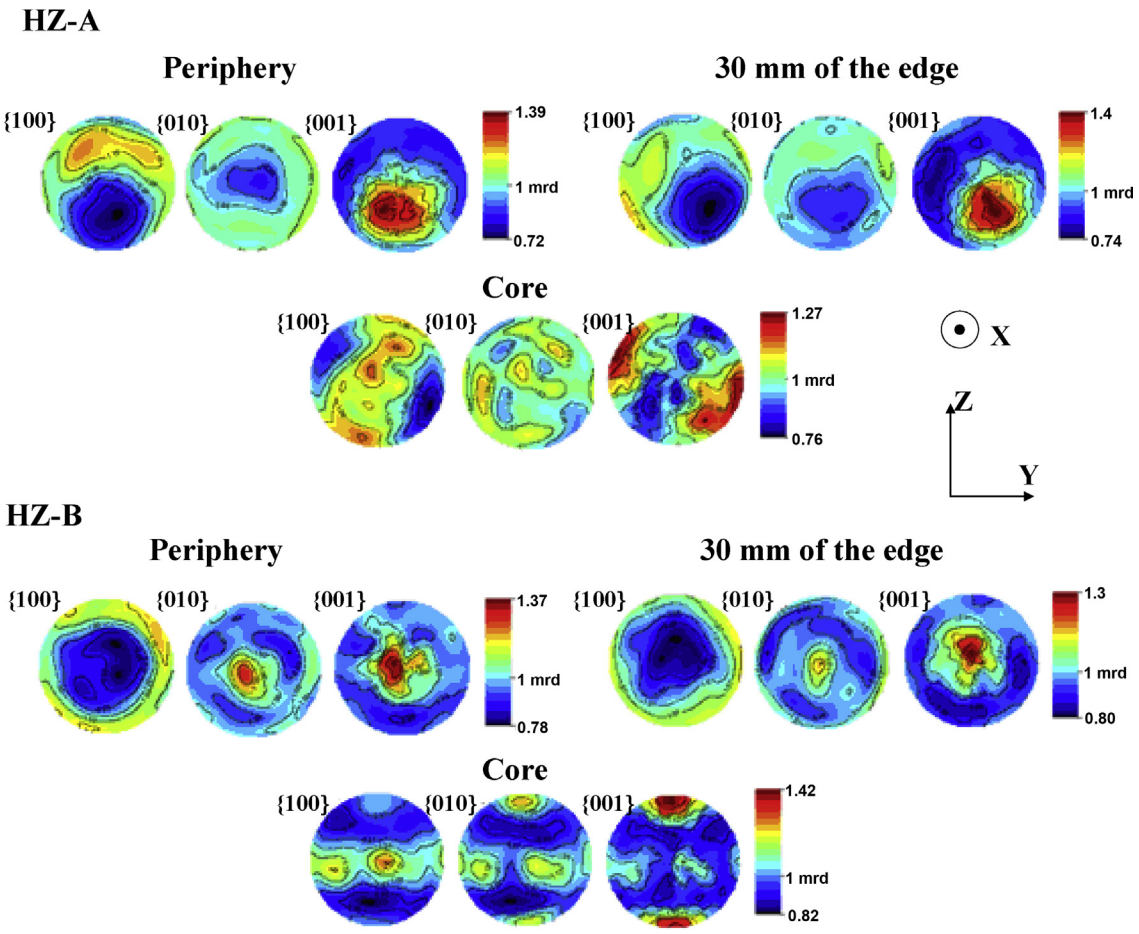

Fig. 8. Pole figures {1 0 0}, {0 1 0} and {0 0 1} for the different samples HZ-A and HZ-B in different sampling zones (*X* axis is normal to the plane of observation).

considering *X* and *Y* as equivalent main direction of thermal gradient. As shown above, these samples may be submitted to a biaxial compression state in the (*Y*, *Z*) plane when passing the T–M transformation. It was shown previously that HZ-A material exhibits a fiber texture along the main direction of thermal gradient *X*. {0 0 1} planes are statistically normal to the direction of thermal gradient, i.e., crystallographic axes $\overrightarrow{c_m}$ are aligned with the main direction of thermal gradient. This texture effect could be a consequence of variant selection during the T–M transformation, induced by a biaxial state of compression

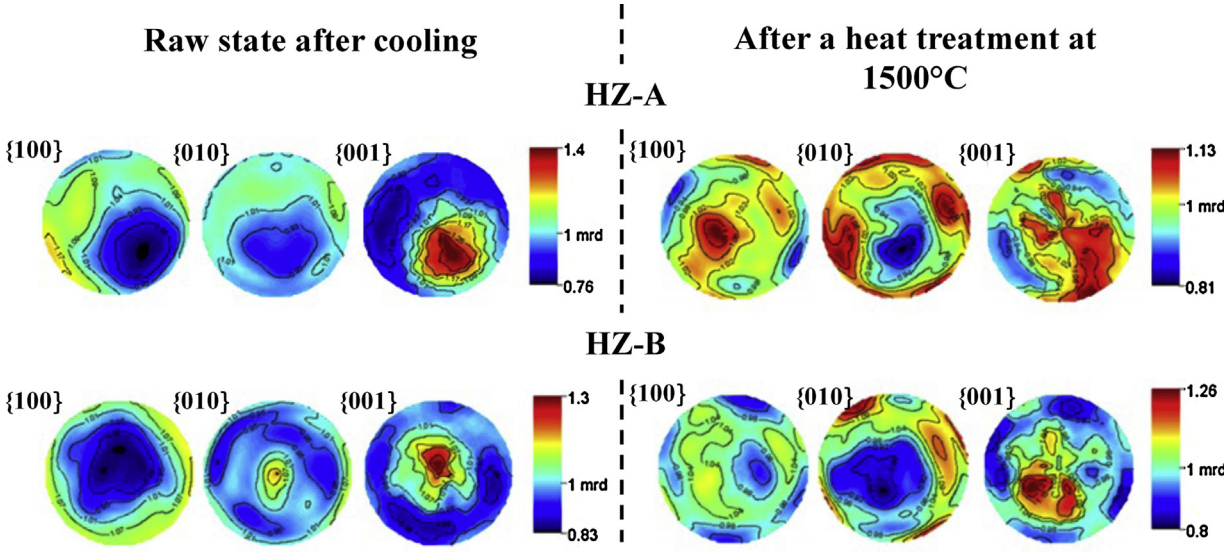

Fig. 9. Pole figures of {1 0 0}, {0 1 0} and {0 0 1} planes after heat-treatment at 1500 °C (sampling at 30 mm of the periphery of the blocks).

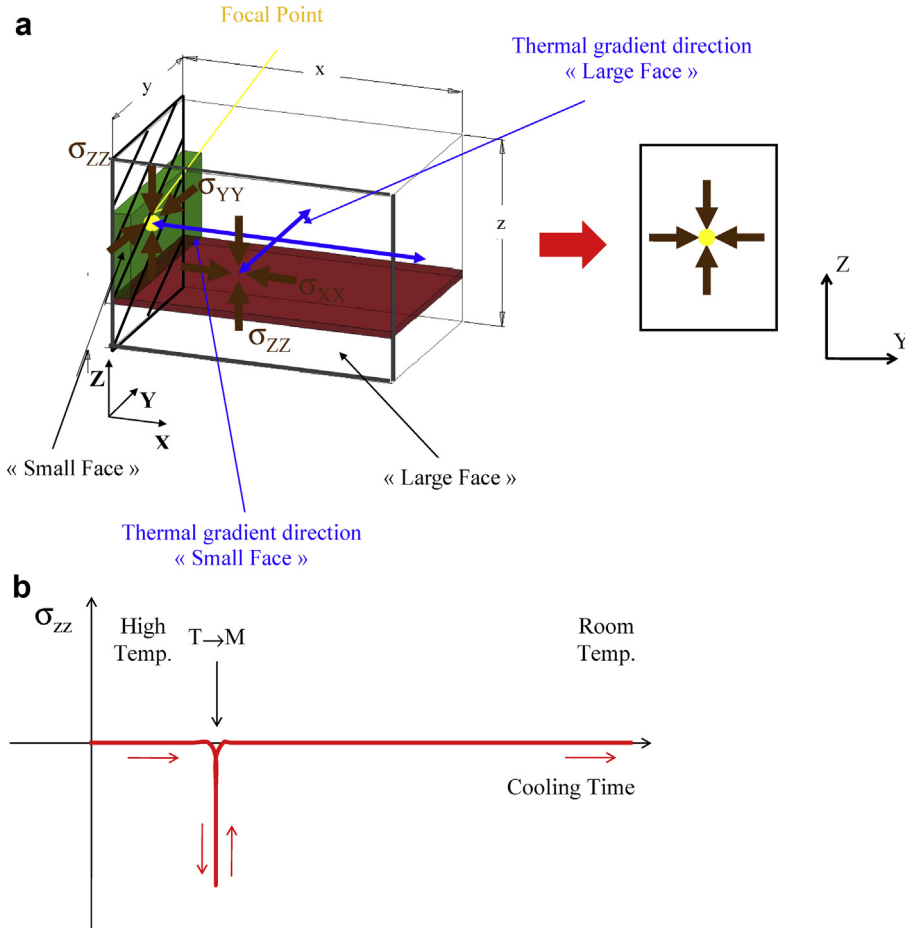

Fig. 10. Schematic of the biaxial compressive state in the (*Y*, *Z*) plane normal to the direction of thermal gradient with a sample from the periphery of the "small face" of the block (a). Evolution of the σ_{zz} mechanical stress during the cooling stage in a zone closed to the periphery of the large face of the block (b) (from[28]).

in the plane normal to the thermal gradient. The crystallographic axis $\overrightarrow{c_m}$ is the larger lattice parameter. Then, a biaxial state of compress ion could potentially create a variant selection during the T–M transition when $\overrightarrow{c_m}$ axis are preferentially oriented outside of the biaxial state of compression. This effect can be assimilated to a selection of variants when a tensile test normal to this plane is applied.

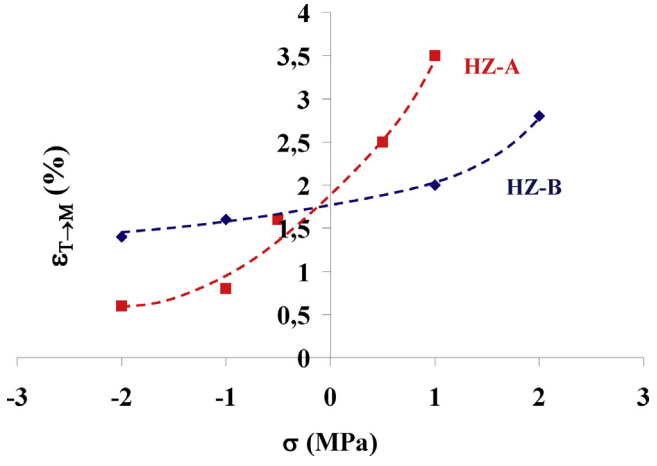

Fig. 11. $\varepsilon_{T\rightarrow M}$ as a function of applied stress during cooling tests for HZ-A and HZ-B.

To reproduce stress field seen by the materials during the casting process, samples were submitted to different levels of uniaxial tensile and compressive stresses when passing the T → M transformation. Strain values related to the martensitic transformation (ε_{T-M}) are plotted in Fig. 11 for the two studied materials. ε_{T-M} strains appear to be stress dependent. Besides, it can be noticed that:

- a tensile stress increases the strain associated to the T–M transformation whereas a compressive one reduces it;
- the effect of tensile stress is strongly marked compared to the compressive one;
- for a given stress, $\varepsilon_{T\rightarrow M}$ produced by a tensile testis higher for HZ-B than for HZ-A.

The $\varepsilon_{T\rightarrow M}$ strain is in concordance with theoretical value seen for polycrystalline zirconia (around 1.76%) when T–M transformation occurs without applied stress.

Analogy between a biaxial state of compression and a tensile stress normal to the plane is proposed here for texture formation. In fact, in both cases, variant selection occurring during the T–M transformation corresponds to an alignment of larger lattice axes ($c_m > b_m > a_m$) with the normal to either the biaxial plane of compression or the parallel to the applied tensile stress. Then, texture

Table 1
Dilatometric changes associated with the M → T transition during a supplementary heat treatment on samples cooled under stress.

Applied stress during previous cooling	$\varepsilon_{M\rightarrow T}$ during a subsequent heating	
	HZ-A (%)	HZ-B (%)
+2 MPa	−2	
+1 MPa	−0.7	−1.5
+0.5 MPa		−1.1
−0.5 MPa		−0.9
−1 MPA		−0.8
−2 MPa	−0.6	−0.5

observed by neutron diffraction in a block submitted to the cooling process may be reproduced in a quite similar way by doing a cooling step with an uniaxial tensile test. Making the hypothesis that the biaxial stress field of compression during the cooling process and the passage of T–M under tensile stress could be analogous, strain associated to M–T ($\varepsilon_{M\rightarrow T}$) of a supplementary heat treatment have been compared to get a qualitative estimation of the stress field during the cooling stage. Table 1 illustrates $\varepsilon_{M\rightarrow T}$ for samples submitted to a supplementary heat treatment from samples cooled under stress.

After a supplementary heat treatment, HZ-A specimens sampled in an area near the edge of the block present higher shrinkage in *X* direction (−1.6% for the peripheric sample and −1.2% for the sample at 30 mm to the edge). This would be in accordance with a state of tensile stresses oriented in *X* direction (−2% for cooling under 2 MPa and −0.7% for cooling under 1 MPa). Obviously, the confrontation of these memory effects remains very qualitative. In reality, the stress field into the block during annealing is more complex than the one resulting from a state of biaxial compression. In addition, the raw samples have not exactly the same thermal history than that experienced by a supplementary heat treatment at 1500 °C followed by a cooling under uniaxial tensile stress. For HZ-B material, the memory effect on the $\varepsilon_{M\rightarrow T}$ deformation is barely visible or absent. The thermal gradient oriented in *X* direction would be less influenced here, when the T → M transformation occurs during the supplementary heat treatment. This result is consistent with both fiber texture planes {0 1 0} and {0 0 1} along *X* observed by neutron diffraction. This texture information indicates that the two crystallographic axes with the most important lattice parameters (c_m and b_m) tend to align with the thermal gradient direction normal to the biaxial compression plane. The lack of memory effect here could be a consequence from a less significant stress field for HZ-B than for HZ-A, during the T → M transition.

It has been shown previously that HZ-B exhibits higher viscoplastic behaviour of the glassy phase compared to HZ-A during the T–M transformation. Fig. 12a and b presents the stress–strain behaviour of both HZ-A and HZ-B during successive tensile-compressive tests curves between 2 MPa and −2 MPa at 20 °C, 750 °C, 950 °C and 1100 °C. The larger strain behaviour of HZ-B appears as an obviousness above 750 °C (which corresponds approximately to the glassy phase transition). Then, internal stresses which exist during the martensitic transformation will be relaxed more easily for the boron-silica

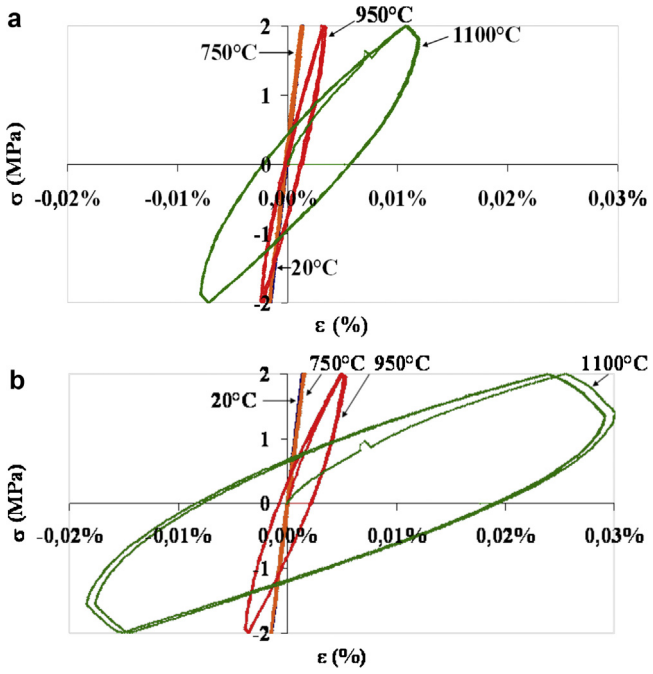

Fig. 12. Stress–strain behavior during tensile-compressive tests between 2 and −2 MPa at 20 °C, 750 °C, 950 °C and 1100 °C for HZ-(A) (a) and for HZ-(B) (b).

glassy phase than for the soda-silica one. This result is in accordance with literature data[29] showing a viscosity reduction effect of boron in silica based glass.

Then stress level is probably much lower for HZ-B than for HZ-A especially during the T–M transformation of the cooling process.

5. Conclusion

Zirconia based refractory blocks face stress field during the cooling process after casting. Two blocks with different chemical composition of the glassy phase have been characterized to evaluate the nature and intensity of texture occurrence in different areas of sampling. Results show that the boron based refractory (HZ-B) exhibits lower texture compared to the soda-based one (HZ-A).

In parallel, tensile-compressive tests were done on HZ-A and HZ-B materials with different stress levels under cooling around the T–M transformation. A relationship between applied stress and strains associated to the T–M transition was highlighted. These tests aim to place materials in analogous stress conditions to the cooling process after casting and to quantify stress levels seen by materials during the cooling process. To evaluate qualitatively this stress field, samples from the block submitted to the cooling process and samples from tensile-compressive tests were submitted to a supplementary heat treatment and strain were measured during the M–T transformation, as a characteristic of their thermal history. It was shown that strain levels are much lower for HZ-B than for HZ-A. This result is consistent with the lower neutron texture of HZ-B and has been associated with the lower viscosity of HZ-B glassy phase.

Acknowledgments

Authors are greatly thankful for the funding of the French National Research Agency and the experimental/human support of the Institut Laue Langevin (ILL-Grenoble-France).

References

1. Patapy C, Gault C, Huger M, Chotard T. Acoustic characterization and microstructure of high zirconia electrofused refractories. *J Eur Ceram Soc* 2009;**29**(16):3355–62.
2. Patapy C, Gey N, Hazotte A, Humbert M, Chateigner D, Guinebretiere R, et al. Mechanical behaviour characterization of high zirconia fused-cast refractories at high temperature: Influence of the cooling stage on microstructural changes. *J Eur Ceram Soc* 2012;**32**(15):3929–39.
3. Massard L. *Etude du fluage de réfractaires électrofondus du système alumine-zircone-silice, Phd, ENSMP*; 2005.
4. Cockcroft SL, Keith Brimacombe J. Thermal stress analysis of fused-cast AZS refractories during production. Part I. Industrial study. *J Am Ceram Soc* 1994;**77**(6):1505–11.
5. Cockcroft SL, Keith Brimacombe J. Thermal stress analysis of fused-cast AZS refractories during production. Part II. Development of thermo-elastic stress model. *J Am Ceram Soc* 1994;**77**(6):1512–21.
6. Thomas BG, Samarasekera IV, Brimacombe JK. Mathematical model of thermal processing of steel ingots. Part II. Stress model. *Metal Trans B* 1987;**18**:131–47.
7. Evans BG, Hutchinson JW, Lu TJ, Srinivasan GV, Winder SM. Stress and strain evolution in cast refractory blocks during cooling. *J Am Ceram Soc* 1998;**81**(4):917–25.
8. Madi K. *Influence de la morphologie tridimensionnelle des phases sur le comportement mécanique de réfractaires électrofondus, Phd, ENSMP*; 2006.
9. Ferry M, Xu W. Microstructural and crystallographic features of ausferrite in as-cast gray iron. *Mater Charact* 2004;**53**:43–9.
10. Rivera G, Calvillo PR, Boeri R, Houbaert Y, Sikora J. Examination of the solidification macrostructure of spheroidal and flake graphite cast irons using DAAS and ESBD. *Mater Charact* 2008;**59**:1342–8.
11. Kriven WM, Fraser WL, Kennedy SW. Advances in ceramics. In: Heuer AH, Hobbs LW, editors. *Science and technology of zirconia*, vol. 3. Colombus, Ohio: Am. Ceram. Soc; 1981. p. 82.
12. Kelly KM, Francis Rose LR. The martensitic transformation in ceramics – its role in transformation toughening. *Prog Mater Sci* 2002;**47**:463–557.
13. Sakuma K. *Microstructural aspects on the cubic – tetragonal transformation in zirconia in Zirconia engineering ceramics – old challenges, new ideas, Key engineering materials*, 153–154. Switzerland: Trans. Tech. Publications; 1998. p. 75–96.
14. Patapy C, Huger M, Guinebretière R, Gey N, Humbert M, Hazotte A, et al. Solidification structure in pure zirconia liquid molten phase. *J Eur Ceram Soc* 2013;**33**(2):259–68.
15. Buljan ST, McKinstry HA, Stubican VS. Optical X-ray single crystal studies of the monoclinic – tetragonal transition in ZrO_2. *J Am Ceram Soc* 1976;**59**(7–8):351–4.
16. Bunge H-J, Wenk H-R, Pannetier J. Neutron diffraction texture analysis using a 2D position sensitive detector. *Text Microstruct* 1982;**5**:153–70.
17. Bunge H-J. *Texture analysis in materials science*. London: P.R. Morris Transactions, Butterworth; 1982.
18. Léon F [Phd] *Développement de l'analyse quantitative de texture utilisant des détecteurs bidimensionnels: application à la texture magnétique*. Université de Caen; 2009.
19. Lutterotti L, Chateigner D, Ferrari S, Ricote J. Texture, residual stress and structural analysis of thin films using a combined X-ray analysis. *Thin Solid Films* 2004;**450**:34–41.
20. Matthies S, Vinel GW. On the reproduction of the orientation distribution function of texturized samples from reduced pole figures using the conception of a conditional ghost correction. *Phys Status Solidi B* 1982;**112**:K111–4.
21. Matthies S, Vinel GW, Helming K. In: Matthies S, editor. *Standard distributions in texture analysis*. Berlin: AkademieVerlag; 1987.
22. Rietveld HM. Line profiles of neutron powder-diffraction peaks for structure refinement. *Acta Cryst* 1967;**22**:151–2.
23. Rietveld HM. A profile refinement method for nuclear and magnetic structures. *J Appl Cryst* 1969;**2**:65–71.
24. Popa N-C. Texture in rietveld refinement. *J Appl Cryst* 1992;**25**:611–6.
25. Chateigner D. Reliability criteria in quantitative texture analysis with experimental and simulated orientation distributions. *J Appl Cryst* 2005;**38**:603–11.
26. Chateigner D. *Combined analysis*. New York: Wiley-ISTE; 2010.
27. Kakroudi MG [Phd] *Comportement thermomécanique en traction de bétons réfractaires: influence de la nature des agrégats et de l'histoire thermique*. Universitéde Limoges; 2007.
28. Laurence L. *Internal Report ANR NOREV, Centre des Matériaux, Mines Paris Tech*. France: Evry; 2010.
29. Haussonne JM, Bowen P, Carry C, Barton J. *Céramiques et verres: principes et techniques d'élaboration*. Presses Polytechniques et Universitaires Romandes; 2005. p. 635–96.